TAL TECH

TALLINN UNIVERSITY OF TECHNOLOGY
SCHOOL OF ENGINEERING
Faculty of Chemical and Materials Technology

DEVELOPMENT OF Sb$_2$S$_3$ THIN FILM ABSORBER BY CLOSE-SPACED SUBLIMATION FOR THIN FILM SOLAR CELLS APPLICATIONS

Sb$_2$S$_3$ ABSORBERKILEDE ARENDAMINE LÄHIDISTANTSSUBLIMATSIOONIL ÕHUKESEKILELISTELE PÄIKESEPATAREIDELE

MASTER THESIS

Üliõpilane:	Sepideh Safdari
Üliõpilaskood:	184647KAYM
Juhendaja:	Dr. Nicolae Spalatu Robert Krautmann

Tallinn 2020

(*On the reverse side of title page*)

AUTHOR'S DECLARATION

Hereby I declare, that I have written this thesis independently.
No academic degree has been applied for based on this material. All works, major viewpoints and data of the other authors used in this thesis have been referenced.

"26" May 2020

Author: Sepideh Safdari /digitally signed/
        /signature /

Thesis is in accordance with terms and requirements

"26" May 2020

Supervisor: Dr. Nicolae Spalatu /digitally signed/
        /signature/

Accepted for defence

"26" May 2020

Chairman of theses defence commission: Prof. Malle Krunks
                                        /name and signature/

THESIS TASK

Student: Sepideh Safdari, 184647KAYM

Study programme,   KAYM Materials and Processes for Sustainable Energetics

main speciality: processes for sustainable energetics

Supervisor(s): Research Scientist, Dr. Nicolae Spalatu, +3726203369

PhD student Robert Krautmann, +37259001250

Thesis topic:

(in English)   DEVELOPMENT OF Sb_2S_3 THIN FILM ABSORBER BY CLOSE-SPACED SUBLIMATION FOR THIN FILM SOLAR CELLS APPLICATIONS

(in Estonian) Sb_2S_3 ABSORBERKILEDE ARENDAMINE LÄHIDISTANTSSUBLIMATSIOONIL ÕHUKESEKILELISTELE PÄIKESEPATAREIDELE

Thesis main objectives:

1. To gain knowledge on principle work of thin film solar cells, thin film deposition methods, and characterisation techniques for studying and analysing thin films and thin film solar cells.

2. To get acquainted with the CSS deposition technique and to deposit thin films by this method.

3. To investigate the influence of CSS deposition temperature on structural and optoelectronic properties of Sb_2S_3 thin film absorber.

4. To analyse the interrelation between Sb_2S_3 absorber structure and Sb_2S_3/CdS device performance.

5. To describe the physicochemical processes responsible for the changes in the Sb_2S_3 absorber and Sb_2S_3 solar cells depending on CSS deposition conditions.

Thesis tasks and time schedule:

No	Task description	Deadline
1.	Deposition of Sb_2S_3 absorber layer on CdS/TCO/glass substrate by CSS technique on different substrate temperatures	
2.	Conducting material characterization techniques to study the impact of CSS deposition temperature on the properties of Sb_2S_3 thin film absorber and Sb_2S_3/CdS thin film solar cells performance	

3.	Evaluation of Solar cell performance via device characterization techniques	

Language: English **Deadline for submission of thesis:** 26th May 2020.

Student: Sepideh Safdari. ….....……........ 26th May 2020.

<div align="center">/signature/</div>

Supervisor: Dr. Nicolae Spalatu   ………………….   26th May 2020

<div align="center">/signature/</div>

Co-supervisor: Robert Krautmann…........................   26th May 2020

<div align="center">/signature/</div>

Head of study programme: Professor Sergei Bereznev   …....................   26th May 2020

<div align="center">/signature/</div>

CONTENTS

PREFACE

Short summary

In this thesis, I investigated the effect of close spaced sublimation (CSS) deposition temperatures, between 260 and 340 ^{o}C, on the properties Sb_2S_3 thin films and Sb_2S_3/CdS thin film solar cells. The structure and morphology of the absorber layer is strongly affected by the deposition temperature. Sb_2Se_3 films with small grains and high density of grain boundaries were obtained at 260 ^{o}C, while compact layers were grown at 300 and 340 ^{o}C. For the later temperature, micro-cracks were detected on the surface of the films. XRD result showed a large number of (120), (130), (230) peaks for the films deposited at 260 and 340 ^{o}C and highlighted (221) peak for the layer obtained at 300 ^{o}C. Evolution of the lattice parameter depending on the deposition temperature indicated presence of in-plane stress in the films, emphasised in the layers grown at 340 ^{o}C. The best PV parameters and efficiency of 2.5% was obtained for the solar cell with Sb_2S_3 deposited at 300 ^{o}C, having dense columnar grains, whereas low performance were achieved for the devices with dispersed Sb_2S_3 films obtained at 260 ^{o}C and cracked Sb_2S_3 layers at 340 ^{o}C.

Keywords: Sb_2S_3 solar cells, thin film solar cells, close-spaced sublimation, solar cell performance, Sb_2S_3 properties.

List of abbreviations and symbols

IRENA International Renewable Energy Agency

PV Photovoltaics

CdTe Cadmium Telluride

CIGS Cadmium Indium Gallium Selenide

α-Si Amorphous Silicon

TF-Si Thin-Film Silicon

CSS Close-Spaced Sublimation

SEM Scanning Electron Microscopy

EDX Energy-Dispersive X-Ray Spectroscopy

XRD X-Ray Diffraction

J-V Current-Voltage

EQE External Quantum Efficiency

TCO Transparent Conductive Oxide

FTO Fluorine Doped Tin Oxide

ITO Indium Doped Oxide

c-Si Crystalline Silicon

CIS Cadmium Indium Diselenide

PCE Photoconversion Efficiency

CBD Chemical Bath Deposition

ALD Atomic Layer Deposition

CSP Chemical Spray Pyrolysis

PVD Physical Vapor Deposition

CdS Cadmium Sulphide

E_g Band Gap Energy

V_{OC} Open Circuit Voltage

FF Fill Factor

J_{SC} Short Circuit Current Density

GBs Grain Boundaries

SEs Secondary Electrons

INTRODUCTION

Global warming and climate change are here, already giving rise to a number of environmental hazards that may eventually have dire socioeconomic impact on hundreds of millions of people. Green energy technologies are seen as one of the many solutions to stop the global warming. According to International Renewable Energy Agency (IRENA), cumulative emissions must at least be reduced by a further 470 gigatons (Gt) by 2050 compared to current situation [1]. Renewable energy use needs to rise at least six times faster in the entire world to start to meet the goals set out in the Paris Agreement [1]. The Paris Agreement's central aim is to strengthen the global response to the threat of climate change by keeping the global temperature rise below 2 degrees Celsius and to pursue efforts to limit the temperature increase even to 1.5 degrees Celsius. [2]

Photovoltaics is regarded as one of the most robust technologies to produce low-carbon power. One of the potential energy sources of the future is solar energy with thin film solar cells. There is extensive research into working on new materials for thin film solar cells, which are low-cost and environmentally friendly [3].

The most common solar cells are silicon based solar cells. Although these solar cells are more available than other types of photovoltaic cells, the amount of material usage in the cells is a major drawback. The thickness of such cells is about 180-300 μm, which forms 52% of the overall cost. As a low-cost, non-toxic, and novel alternative, thin film solar cells are introduced [4]. A direct band gap and high absorption coefficient are the two most important properties for a material to be chosen as a candidate for employment in thin film solar cells. The mentioned properties increase the amount of light absorbed by the cell and as a result, increase electricity production. Thin film solar cells usually possess a thickness of 1-5 μm and they can be deposited on different substrates such as plastic, steel or glass [4]. Various kinds of thin film solar cells are being manufactured, including cadmium telluride (CdTe), copper indium gallium di-selenide (CIGS), and amorphous thin-film silicon (a-Si, TF-Si) [5]. Even though these cells are commercially available, the toxicity of Cd and rarity of In and Te along with high cost of In and Ga, are barriers for continuous production [4].

In this thesis, we investigate the effect of different substrate temperatures on Sb_2S_3 absorber layer film growth, which has been deposited on substrate by close-spaced sublimation (CSS) method. Sb_2S_3 is a cost-effective, non-toxic, and earth abundant, photovoltaic material with a bandgap of about 1.7 eV [6]. The CSS method used in this

experiment is a physical vapor deposition technique for depositing Sb_2S_3 absorber material, as it can form large grains in the absorber structure, which consequently decreases the concentration of grain boundaries [4].

This study comprises of three major chapters. First, I will introduce the physical principle of solar cells, followed by the description of thin film solar cells and properties of Sb_2S_3, and the explanation of the deposition method. Following the mentioned sub chapters, I am first going to give a description of characterization methods [4]. Material characterization techniques include scanning electron microscopy (SEM), energy-dispersive X-ray spectroscopy (EDX), X-ray diffraction (XRD), and van der Pauw measurement. Sb_2S_3 solar cells performance was measured by current voltage (J-V) characteristic and external quantum efficiency (EQE). Secondly, the experimental part describes the Sb_2S_3 deposition and finally the result and discussion part explains the effect of substrate temperature on the Sb_2S_3 film growth and the efficiency of Sb_2S_3 solar cells.

1. THEORETICAL BACKGROUND

1.1 Solar cells

Solar cell (photovoltaic cell) is a device that transforms light into electricity. The cell is made of semiconductor materials, which enables charge generation and separation upon photon absorption to produce electricity. There are different layers in a solar cell, such as glass, TCO, buffer layer, absorber layer and finally the back contact. Solar cells are connected together in series or in parallel to create a solar panel.

1.1.1 Solar cells working principle

As mentioned above, a solar cell is an electrical device that converts the solar energy into electrical energy through the photovoltaic effect.
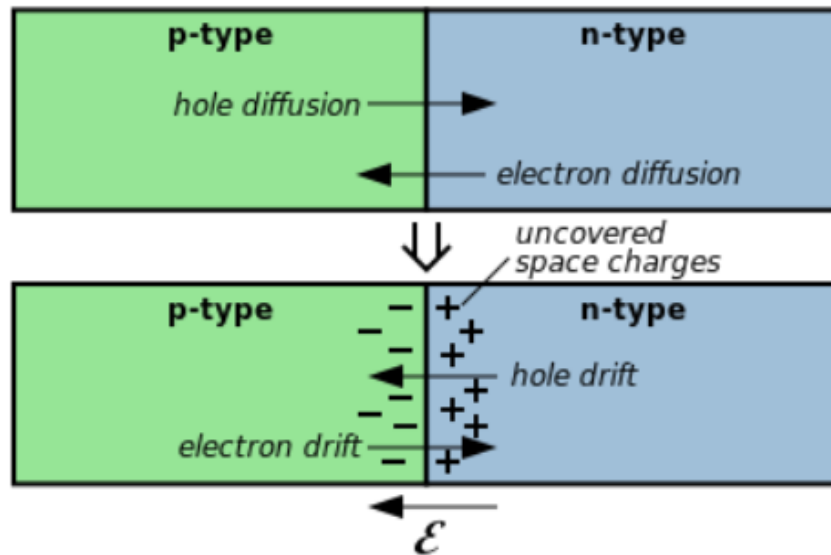
Figure 1. Formation of p-n junction and occurrence of the internal electric field [3].

The first layer is glass, which has the purpose of keeping the cell from getting contaminated. Glass is coated with a transparent conductive oxide (TCO), usually either fluorine doped tin oxide (FTO) or indium doped oxide (ITO) are being used. The purpose of TCO is to act as front contact, which collects electrons and transfers them to an external circuit. Then comes the window layer, which has n-type conductivity Next comes the absorber layer, in this study it is Sb_2S_3 that has p-type conductivity. When p-type and n-type semiconductors are placed next to each other, they establish a p-n junction (Figure 1). The n-type layer has the excess of electrons and the p-type layer has the excess of holes. Electrons in the n-type layer diffuse to the p-type layer and the holes from p-type layer diffuse into the n-type layer. Because these two layers have opposite charges, an electric field forms that prevents subsequent diffusion. Then a p-n

junction establishes an electric field, which makes sure charge carriers move in a certain path [3]. The back of the absorber is coated with a back contact, which collects holes and transfer them into external circuit.

Solar cell only produces energy, if the incident solar photons have enough energy to excite electron-hole pairs. If the absorbed photon energy is equal or above the band gap energy of the absorber, the electron is excited to conduction band and becomes a mobile carrier that is then swept to external circuit by the p-n junction. The electrons then move through a circuit, lose their energy as electricity, and return to the cell through the back contact, where they recombine with a hole. This cycle of events ceases once there is no longer illumination.

There are various types of photovoltaic cells using different materials as the absorber. The most commonly used solar cell is crystalline silicon (c-Si) that owns 90% of PV technology production today. However, due the high amount of material used in silicon solar cells, the cost of such cells is high. Thus, thin film solar cells such as Sb_2S_3 could be a cheaper alternative if it achieved same efficiency for a cheaper manufacturing cost [5].

1.1.2 Thin film solar cells

Thin film solar cells are the photovoltaic cells that employ absorbers that have a thickness of 1-5 μm [3]. In addition, they can be deposited on different types of substrates, such as glass, plastic and metal. Their lower material consumption is one potential advantage over silicon based solar cells along with higher absorption ability, flexibility and lightweight, are key properties that makes these cells attractive for future energy production. Commercially available thin film solar cells are amorphous silicon (a-Si), cadmium telluride (CdTe), copper indium diselenide (CIS), copper indium gallium diselenide (CIGS) [5].

1.1.3 Sb_2S_3 absorber layer

Numerous earth-abundant, non-toxic materials for solar cells are being investigated. Compounds such as $Cu_2ZnSn(Se,S)_4$, $Sn(Se,S)$, $Cu_2Sn(Se,S)_3$, Cu_2O, $CuSbS_2$, Cu_3N, FeS_2, $Cu_2BaSn(Se,S)_4$, and $Sb_2(Se,S)_3$ have been researched as potential photovoltaic absorbers. The commercialization of these solar cells is however not yet viable due to low power conversion efficiencies (PCE) as compared to the conventional PV technologies [7].
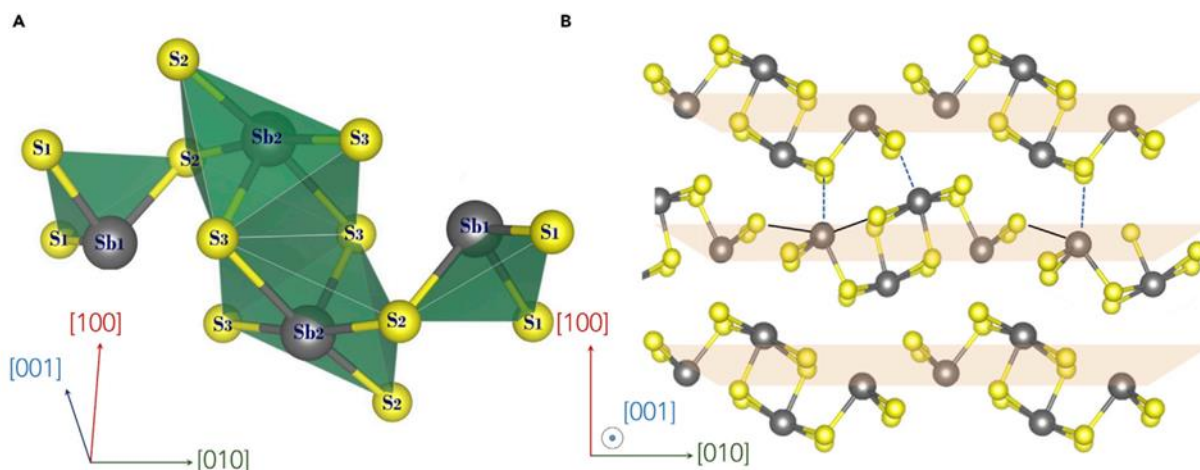
Figure 2. Crystal structure of Sb₂S₃

(a) Single (Sb₄S₆)ₙ Showing two trigonal and two square pyramid Sb atom coordination.

(b) View of SbS₃ crystal structure projected on (001) plane. Grey spheres are Sb and yellow are S atoms. solid lines are bonds between separate ribbons and dashed lines show bonds between the sheets [7].

As to commercially available thin film solar cells, their market expansion has not realized due to somewhat higher solar cell price. Furthermore, the issues of availability (In, Te) and toxicity (Cd) of certain elements has made the scientific community look for cheaper and non-toxic materials [8].

Antimony trisulfide (Sb_2S_3) is a potential photovoltaic absorber material because it possesses a high absorption coefficient ($\alpha > 10^4$ cm^{-1}) [7], along with a desired bandgap. Previous studies have reported differing band gap values. Kondrotas et al. reported 1.7-1.8 eV [7], Zeng et al. 1.7 eV [11], Guo et al. 1.7 eV [6], Messina et al. 1.88 eV [12], Nair et al. 1.5-1.8 eV [9], Eensalu et al. 1.7 Ev [13], Versavel et al. 1.73 eV [8], and Wang et al. 1.7 eV [10]. The band gap range of 1.6–1.8 eV is well suited for photovoltaic application [9].

Sb_2S_3 structure consists of $(Sb_4S_6)_n$ arrays(ribbons) that grow along the [001] crystal direction. Each ribbon is comprised of two trigonal SbS_3 and two square SbS_5 pyramids creating a primary building block in Sb_2S_3 crystal (Figure 2A). Ribbons are then attached together and create zigzag sheets perpendicular to a (100) plane (Figure 2B). Totally, the bond length of Sb-S, d, in Sb_2S_3 can be listed into three classes: along the [001]

direction (d < 2.5 A°), along the [010] direction (2.58 < d < 3.25 A°, Figure 2B, solid line), and along the [100] direction (3.45–3.74 A°, Figure 2B, dashed line). Then, there's a strong covalent bonding in ribbon along the c-axis, but ribbons and sheets atoms are attached together via weaker bonds, especially in the [100] direction. This is certified by experimental inspections that show single crystals are simply cleaved in the direction perpendicular to the (100) plane [7].

Sb_2S_3, can be deposited onto the different substrates by various techniques. Some of these techniques are chemical bath deposition (CBD), spin coating, atomic layer deposition (ALD) or chemical spray pyrolysis (CSP) method, and physical vapor deposition (PVD) [13].

The most used technique for depositing Sb_2S_3 is chemical bath deposition (CBD). The advantages of this technique are fast deposition and low cost, although difficulty in controlling the crystal growth in this method along with purity of the final sample are its drawbacks. In addition, post-heat treatment is needed to grow crystalline Sb_2S_3. In wet chemistry methods like CBD, due the mentioned disadvantages of the method, controlling the thickness and purity of the final sample is much more difficult compared to physical vapor deposition methods [11].

In this work, we develop a close-spaced sublimation (CSS) method to grow Sb_2S_3. CSS technique, is mostly used in manufacturing CdTe solar cells. Like CBD, the CSS method also has fast deposition time, although, in CSS the purity control along with stability are ensured. The films produced by this technique are compact and uniform and the crystal growth is extended through the whole film [11].

In particular, there is a need for a rapid deposition technique, which could give us the ability to control the temperature of the source and the substrate, in this case CSS method has the lead. The source is directly vaporized and deposited on the substrate. The CSS technique lowers the cost of the process and unlike the CBD technique, can improve the the quality of the deposited material. Recently, this technique, has been used in manufacturing Sb_2Se_3 as a thin film absorber with an achieved PCE of 6.8% [6]. In recent years, Sb_2S_3 has attracted the attentions to itself due to its plain structure and production [10]. Sb_2S_3 has been used in low thickness absorber solar cells due to its great absorption coefficient in the visible light spectrum (1.8×10^5 cm^{-1} at 450 nm) [13].

1.1.4 CdS window layer

Cadmium sulfide (CdS) is a semiconductor material used in solar cells as the window or n-type layer. The desired bandgap (2.5 E_g) and great transparency (>80%) of this material, makes it a considerable choice as n-type layer [4].

Various methods are used to deposit CdS, such as Close spaced sublimation (CSS), physical vapor deposition (PVD), and chemical bath deposition (CBD), and among all, CBD is the most used deposition technique, due to simplicity and low cost. As a disadvantage, CdS has an amount of toxicity, and there needs to be a new replacement for this material in the future [4].

The light photons absorbed by the CdS layer produces a small amount of photocurrent, which affects the quantum efficiency at wavelengths that are less than CdS band gap. However, with decreasing the thickness of the layer, this issue might be solved [14].

1.2 Deposition technique

1.2.1 Close spaced sublimation (CSS)

Physical vapor deposition methods are superior to other methods due to their considerable features. There is no chemical wasted in the process, along with the ability to keep toxic or flammable gases away comparing to wet chemistry methods. One of the methods of PVD techniques is CSS. CSS is one of the most beneficial and simplest methods in PVD that allows the deposition of low evaporation temperature semiconductor materials [15]. Semiconductors with evaporation temperature below 800 °C, can be deposited on different substrates in vacuum and atmospheric pressure conditions. The source material is in solid form, usually in a powder shape or chunk [15].

The source material is heated to the temperature of evaporation. The vaporized material is moving towards the substrate, and being deposited on the substrate which usually has a lower temperature than the source material. The process condition is in vacuum, which prevents the contamination of the source or the substrate. In this case, the final sample is of high purity. Closed-spaced sublimation system is shown in Figure 3 [4] [5]. In the CSS technique, the distance between the source and the substrate is small (usually less than 1 mm) [16].
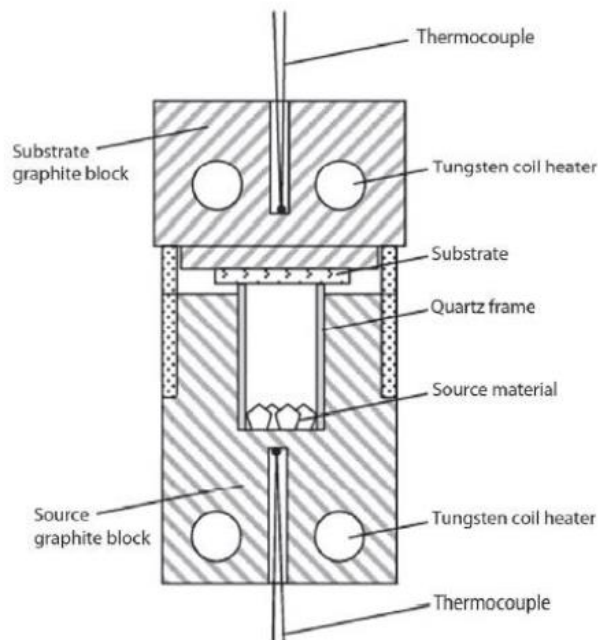
Figure 3. Schematic diagram of close spaced sublimation system [5].

In particular, the CSS technique is used for the deposition of dense planar thin films, as it benefits from high deposition rates and can be easily scaled up for module manufacturing [17].

1.3 Characterization techniques

1.3.1 Scanning electron microscopy (SEM)

Scanning electron microscopy (SEM) is a technique for analyzing the surface of the sample [18]. Different structural and topological properties of the material such as grain size and orientation along with film thickness are being obtained by this technique [4]. In this technique, a thin electron beam is used for obtaining high quality images of the sample topography. The electron beam strikes the sample and the backscattered electrons emitted from the surface of the sample, form the image. As the electron beam used in this process is quiet narrowed, the final images have a high depth of field that is used for study of the sample's topography [19]. Figure 4 shows the layout of an SEM microscope, which includes the electron gun (electron source and accelerating anode), electromagnetic lenses for electrons focus, a vacuum chamber covering the sample surroundings, and a number of detectors for collecting the scattered electrons coming from the sample [18].
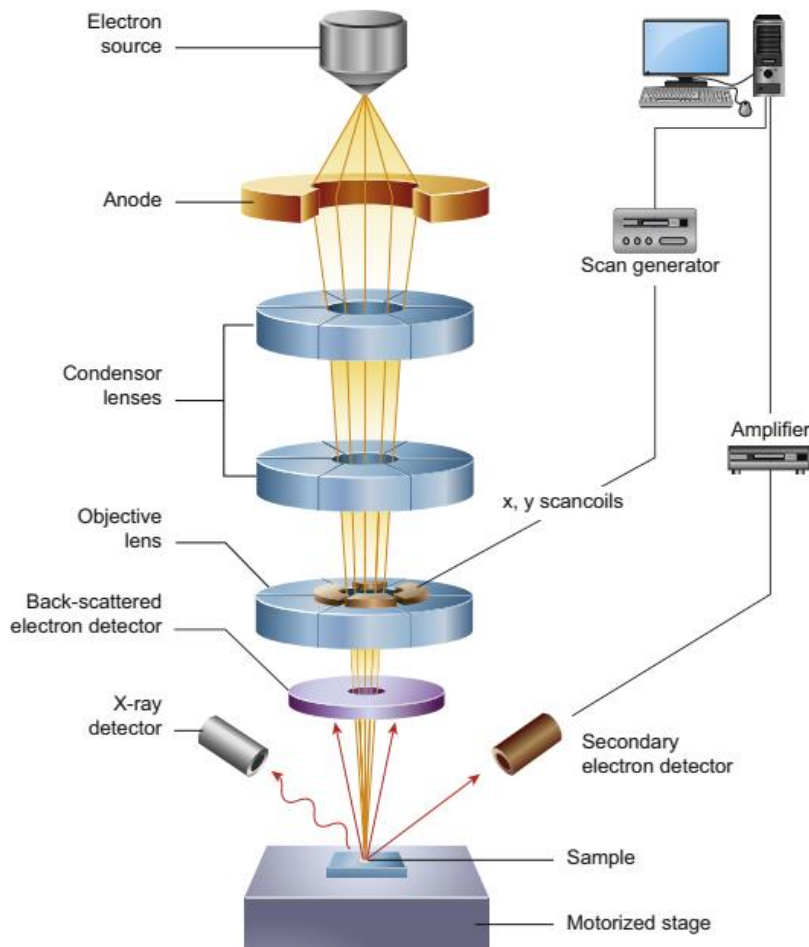
Figure 4. Schematic diagram of the main components of an SEM microscope. [18]

SEM uses an electron emission, which strikes the sample. This strike happens in the electron gun. A filament in the gun is heated by an electric field, and then the anode will send the electrons rapidly towards the sample. Electromagnetic lenses focus the electron beam reaching the sample, which has a narrow diameter about 1 nm [3].

When the electron beam emitted from the electron gun will hit the sample, the electrons can scatter back and create the secondary electrons or X-rays. Secondary electrons (SE) are used to investigate the sample surface and cross-section. Secondary electrons are produced, when incident electron forces out an inner shell electron of the sample's atom. The energy of the SEs are low, about 2-5 eV, due the loss of energy because of the impact [4].

The amount of SEs emitted electrons relies on sample topography. The secondary electrons are detected by a positively charged detector, which is located around the microscope column, and as they hit the surface of the sample it shows topological properties and an image of the surface of the sample [3].

1.3.2 Energy-dispersive X-ray spectroscopy (EDX)

EDX is a detector that is placed in a SEM device and is able to analyze the local elemental composition of thin films. Electrons interact with atom's inner shell electrons that results in the inner shell electron dislodgement from atom's electron cloud. In this process, holes are created which gives the second shell electrons a chance to fill them. In this case, the potential energy difference between the outer and inner shells of the electron is emitted as X-ray. The emitted X-ray gives the possibility to analyze the elemental composition of the material under study. The EDX scheme can be seen on Figure 5 [3].
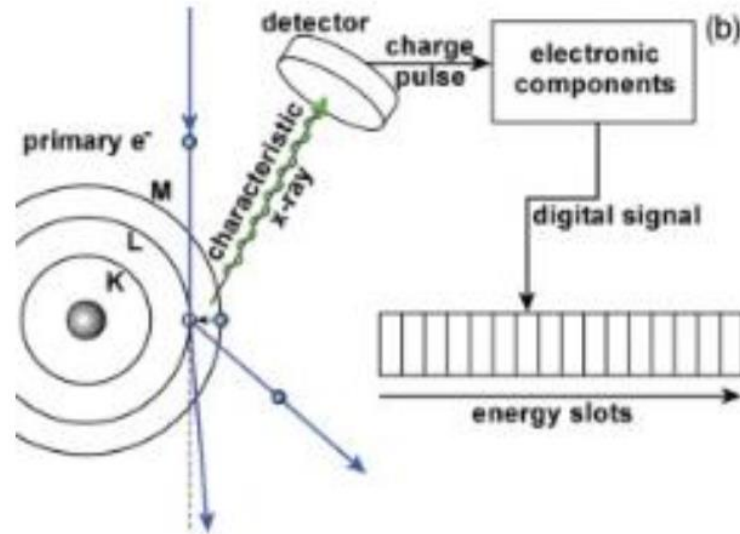
Figure 5. Schematic of EDX [3].

Energy-dispersive uses a white beam (polychromatic beam over the complete available wavelength range) that detects the diffraction peaks at a steady 2q angle by using energy-resolved detectors. In here, the Bragg's law needs to be modified as given in eq. 1:

$$Ehkl = n \times \frac{h \times c}{2 \times \sin \theta} \times \frac{1}{dhkl} \quad (1)$$

One advantage of this technique is that detector movement is not essential for capturing a large number of peaks. As a result, in situ fast measurements can be done with this method. Another advantage is changeable penetration depth of the signal due to the broad energy range in reflexing mode measurements. Because of this characteristic, the varying diffraction peaks at different energy levels can be given to different depth positions, and therefore analysis of depth of the sample can be carried out without elimination of the material and without sample or detector being replaced. One of the main applications of this method is the analysis of the depth-resolved residual stress [20].

1.3.3 X-ray diffraction (XRD)

X-ray diffraction (XRD) is a nondestructive characterization technique, used for analyzing the structure, phases, lattice parameters and crystal orientations of a crystalline material, as well as grain size and crystal defects [21]. When atoms are arranged together in a specific crystal orientation, they create a crystal plane. X-ray beams that scatter from these crystal planes and interfere constructively give the X-ray

diffraction peaks [4]. X-ray diffraction peaks are created when constructive beam of X-rays hit the surface of the sample and being scattered back in different specific angles to a detector which is located into the X-ray device [3][4][21]. Many times the emitted beams interfere destructively, but in cases that the scattered beams are non-destructive, the peaks are obtained. Diffraction of X-rays is given by Bragg's equation [3].

$$n\lambda = 2d.\sin\theta \quad (2)$$

Where λ is X-ray wavelength, d is inter-planar distance, θ is angle of incidence with lattice plane and n is integer [3].

Bragg law expresses that when the phase difference is an integer number of wavelengths, two X-rays, scattered from two consecutive crystal planes, interfere constructively [4].

The atoms positions in the crystal planes determines the peaks of the material. These peaks are considered as material fingerprint showing the orderly arrangement existing in the material. With an online research in the standard database for X-ray diffraction patterns, the phase identification of the samples can be determined easily [21]. Figure 6 depicts the schematic of Bragg-Brentano X-ray diffraction scan, where X-rays are detected in the detector placed in the device [4].
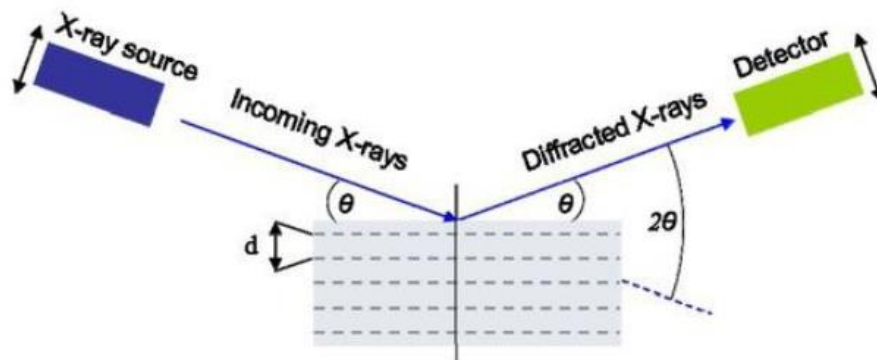
Figure 6. Schematic of an X-ray diffraction scan [4].

It is shown in the picture that incoming X-rays and diffracted X-rays both have the same angle with the crystal plane.

1.3.4 Van der Pauw measurement

The Van der Pauw measurement is a method for precisely measurement of resistivity of a sample. This technique also allows for other properties of materials to be obtained such as resistivity, doping type, sheet carrier density and mobility [22].

In Van der Pauw method, there is a four-point probe, which is shown in Figure 7. the measurement in this method is done using the four mentioned probes. The middle probes are used to pass a small current, while the outer probes measure the voltage. resistivity can be calculated by Equation 3 [4]:

$$\rho = Rsq \times d \ (3)$$

Where d is film thickness in cm, ρ is the film resistivity in $\Omega \cdot cm$, R_{sq} is the sheet resistance under illumination in $\Omega \ sq^{-1}$ [4].
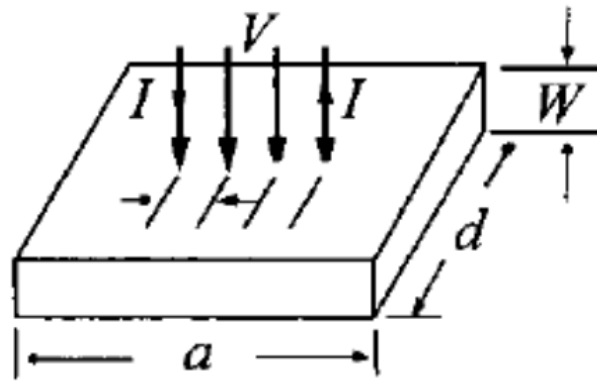
Figure 7. Schematic of four-point probe configuration, where small current is passed through inner two probes, while outer two measure voltage [4]

1.3.5 Current-voltage (I-V) characteristic

Current-voltage (I-V) curve characteristic shows how well the solar performs. Solar cells work like diodes owing to the pn-junction. But unlike usual diodes, solar cells produce photocurrent and generate photo voltage under illumination. Solar cells can be characterized by the I-V curve characteristic. Figure 8 displays a typical I-V curve of a solar cell. The main photovoltaic parameters, which are extracted from the I-V curve, are the short circuit current (J_{SC}), open circuit voltage (V_{OC}), fill factor (FF) and power conversion efficiency (PCE).
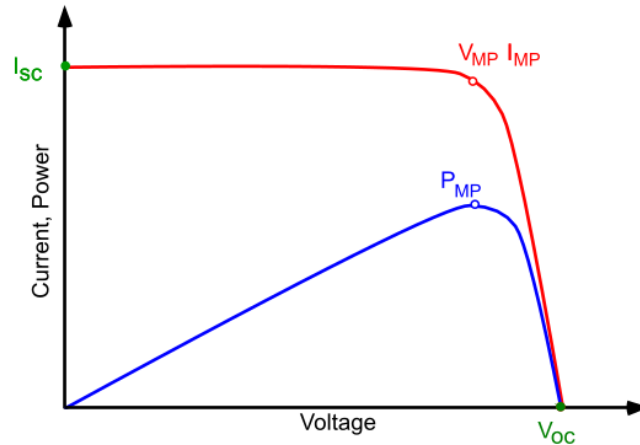
Figure 8. I-V curve of a solar cell. The maximum power point of the solar cell is extracted from the maximum power point [23].

The short circuit current is the maximum photocurrent the solar cell produces in the short circuit condition. Usually, the photocurrent is shown as short current density (J_{SC}), where the current is divided by the contact area. Open circuit voltage is the voltage the solar cell achieves, when it is in an open circuit. For an ideal solar cell, the IV-curve would have a rectangular shape. Field factor shows how the measured I-V curve compares to an ideal I-V curve. Photo conversion efficiency shows the ratio of produced electrical power to the incident solar power. Higher is the efficiency, more light has been harvested for producing electrical power.

The maximum power of a solar cell is extracted from the maximum power point. This refers to the point on the I-V curve, where the product of the J_{SC} and the V_{OC} is the largest. Knowing the maximum power, the photo conversion efficiency is found as follows:

$$PCE = \frac{I_{mp} \times V_{OC}}{P_S}$$

where J_{mp} is the maximum point for short circuit current density in mA cm^{-2}, V_{OC} is the maximum point for open circuit voltage in V and P_S is the solar irradiance in mW cm^{-2}.

1.3.6 External quantum efficiency (EQE)

The measure of ability of a photovoltaic device to convert solar energy to electrical current is called External Quantum Efficiency (EQE) [23]. The more the number of captured incident photons, the more the EQE, thus, EQE amount determines the workability of a solar cell [4] [23].
Figure 8 shows the theoretical and actual EQE amounts expected at all wavelengths [23].
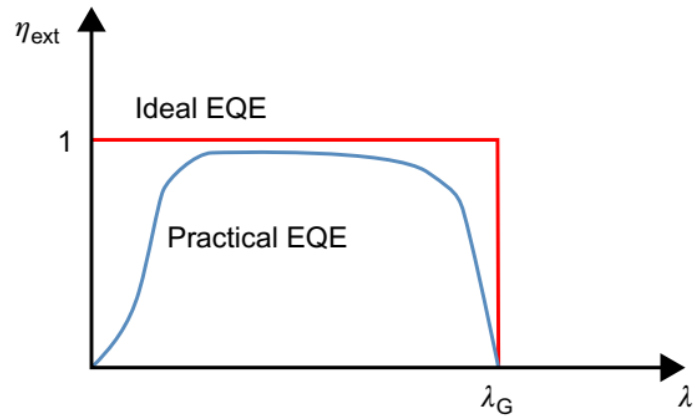
Figure 8. Ideal and practical EQE of a solar cell [23].

When ideal and practical lines are closer to each other, the ability of the solar cell to produce electricity from light photons increases.

1.4 Summary of theoretical background and aims of the thesis

According to the theoretical background presented in the literature overview, the followings are the summary of the literature above:

1) Solar cell is a photovoltaic device that converts the energy of sun light into electricity. There are different types of solar cells, the most common is the silicon based solar cell, followed by the second generation, which are the thin film solar cells. A solar cell is a stack made from different layers with each layer having its specific function. In our structure, the ITO-coated glass serves as the front contact and the substrate onto which subsequent layers, namely the window layer CdS, the absorber layer Sb_2S_3. and the Au back contact were deposited.

2) Sb_2S_3 is an emerging photovoltaic material due to high absorption coefficient ($\alpha > 10^4$ cm^{-1}) and suitable bandgap in the range of 1.6–1.8 eV. It is a non-toxic compound with earth abundant elements and a single orthorhombic structure. These properties make Sb_2S_3 attractive as a potential photovoltaic absorber.

3) CSS technique is a physical vapor deposition method, in which a thin film is obtained by rapid sublimation of respective material powder. In this study, CSS method is used to deposit both the window layer CdS and the absorber layer Sb_2S_3. CSS deposition is carried out in vacuum to achieve higher purity films and faster deposition rate. CdS is used as the window layer. As a n-type semiconductor, CdS has high bandgap (E_g = 2.5) and is highly transparent (>80%) to visible light.

4) There is a limited number of studies in literature on the development of Sb_2S_3 films and Sb_2S_3/CdS solar cells by CSS. Systematic investigations are required to use the advantages of Sb_2S_3 PV novel material for next generation efficient solar cells.

5) There are various characterization methods in this study to investigate the properties of the materials and the solar cell devices. Morphology and crystal growth of Sb_2S_3 films are characterized by SEM and EDX. Sb_2S_3 crystal structure is analyzed by XRD. Van der Pauw method is used to measure the resistivity of the films. IV-curve and EQE measurements are made to evaluate the Sb_2S_3 solar cell performance.

Based on the literature overview, the aims of the thesis are:

1) To gain knowledge of the work principle of thin film solar cells, thin film deposition methods, and characterization techniques for studying and analyzing thin films and thin film solar cells.

2) To get acquainted with the CSS deposition technique and to deposit Sb_2S_3 thin films.

3) To investigate the influence of CSS deposition temperature on structural and optoelectronic properties of Sb_2S_3 thin film absorber.

4) To analyze the relationship between the Sb_2S_3 absorber structure and Sb_2S_3/CdS solar cell device performance.

5) To describe the physicochemical processes responsible for the changes in the Sb_2S_3 absorber and Sb_2S_3 solar cells depending on CSS deposition conditions.

2. EXPERIMENTAL

2.1 Sb$_2$S$_3$ solar cell fabrication

We used soda-lime glass substrates coated with a 200 nm thick 25 Ω sq^{-1} fluorine-doped tin oxide (FTO). Substrates were immersed into a 10 g K$_2$Cr$_2$O$_7$ + 10 mL H$_2$0 + 100 mL H$_2$SO$_4$ solution for 2-3 h at room temperature, after which substrates were rinsed with deionized water and dried in air. CdS buffer films were deposited via close-spaced sublimation (CSS) onto freshly cleaned substrates. Source material, laid on the bottom of CSS system, was solid CdS in powder form (99% wt) purchased from Sigma-Aldrich. The FTO substrate was fixed on a graphite support, facing the source material at the distance of 11 mm. Mechanical and diffusion pumps were used to reach vacuum level of 10^{-4} Pa. Source and substrate graphite supports are equipped with separate heating filaments. The substrate temperature was varied from 260 to 340 ^{o}C while the source temperature was kept constant at 450 ^{o}C. The 450 ^{o}C source temperature was chosen to allow a deposition rate of $\sim$ 1-1.5 µm/min. Throughout the deposition period, both source and substrate temperature were held constant. Sb$_2$S$_3$ absorber films were deposited also via CSS onto the FTO/CdS substrates. Source material used was solid Sb$_2$S$_3$ in powder form (99% wt) purchased from Sigma-Aldrich. Then, gold back contacts of 25 mm^2 size were vacuum evaporated under a vacuum pressure of 10^{-3} Pa.

2.2 Material and device characterization

Top-view and cross-sectional images of layers were made by Zeiss EVO-MA15 scanning electron microscope (SEM) equipped with a Zeiss HR FESEM Ultra 55 system. X-ray diffraction (XRD) patterns were recorded using a Rigaku Ultima IV diffractometer with Cu Kα radiation (λ = 1. 54 Å, 40 kV, 40 mA). J-V curves were measured using an AUTOLAB PGSTAT 30 and an Oriel class A solar simulator 91159A (100 mW cm^{-2}, AM1.5) in air ambient at room temperature. EQE of solar cells was measured using the light source generated by a 300 W xenon lamp and then split by a SPM-2 Carl Zeiss-Jena monochromator working at 30 Hz.

3. RESULTS AND DISCUSSION

Section 3.1-3.2 describe the results of investigation on the influence of CSS deposition temperature on structural and optoelectronic properties of Sb_2S_3 thin film absorber and Sb_2S_3/CdS solar cells. The focus is on screening and optimization of CSS deposition conditions towards development of compact, pinhole-free, and homogeneous Sb_2S_3 absorber layers and efficient Sb_2S_3/CdS thin film solar cells. Interrelation between Sb_2S_3 absorber structure and device performance are discussed and analyzed and physicochemical processes responsible for the changes in the Sb_2S_3 absorber and Sb_2S_3 solar cells are proposed.

3.1 Impact of CSS deposition temperature on the properties of Sb_2S_3 thin film absorber layers

To study the effect of CSS deposition (substrate) temperature on the structural and morphological properties of the Sb_2S_3 thin films, a large series of Sb_2S_3 thin films (~ 30 samples) were deposited onto CSS-CdS/FTO/glass substrates (following the superstrate configuration) whereas the substrate temperature was varied from 260 to 340 °C while the source temperature was kept constant at 450 °C. The 450 °C source temperature was chosen to allow a deposition rate of ~ 1-1.5 μm/min. The changes in the thin film properties were investigated by XRD and SEM. Figure 9 shows the top- and cross-sectional-view SEM images of the Sb_2S_3/CdS/FTO/glass samples with Sb_2S_3 absorber layer deposited at temperatures of 260-340 °C. As can be seen, the Sb_2S_3 grain shape and size greatly depend on the CSS substrate deposition temperature with a clear tendency of grain size increase with the increase of the deposition temperature from 260 to 340 °C. The films deposited at 260 °C consisted of plate shaped small grains (Figure 9a-c), a porous structure with high density of grain boundaries (GBs) (Figure 9a). The growth followed the same features which were previously observed in CdTe and Sb_2Se_3 thin films deposited by CSS at low substrate temperatures [4][5][24][25]. Sb_2S_3 layers grown at 300 °C exhibit a dense structure with long, large and sintered grains (Figure 9b). By increasing the substrate temperature from 300 to 340 °C, the grain size increased considerably (Figure 9c), the density of GBs decreased, resulting in films with a close packed morphology (Figure 9c). At the same time, at 340 °C an interesting effect has been observed where several micro-cracks were clearly detected on the surface of the Sb_2S_3 films (Figure 10).
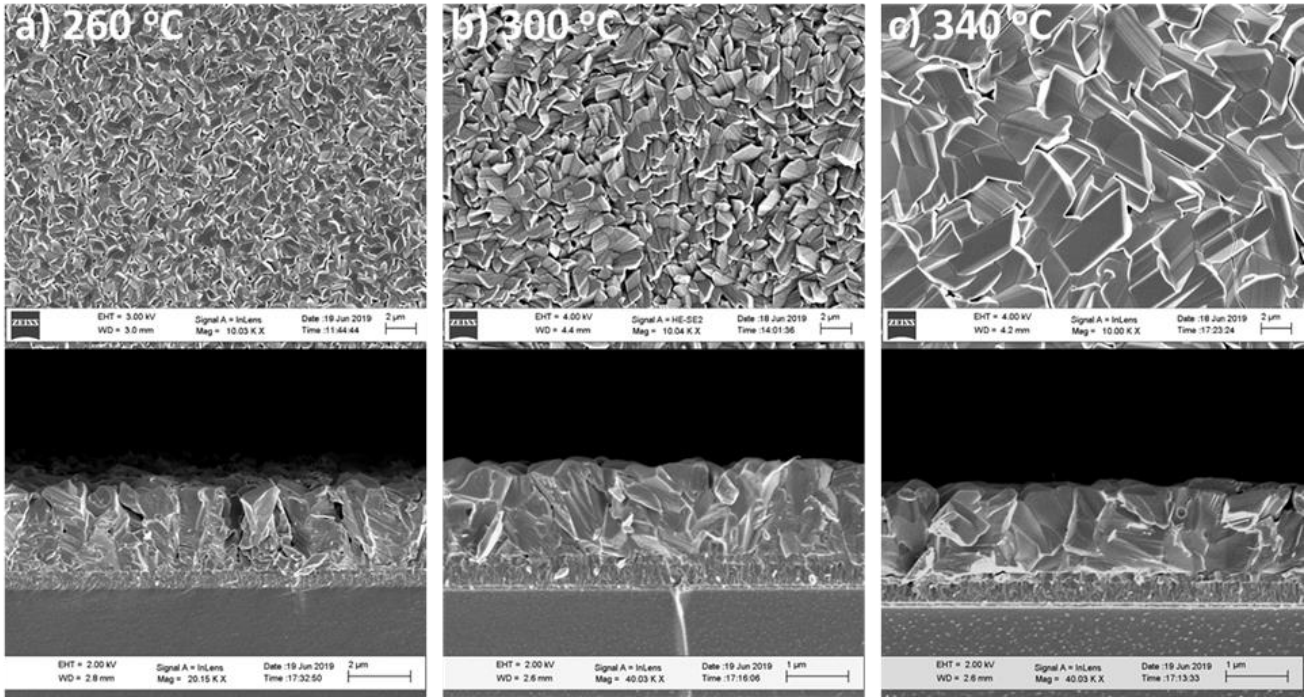
Figure 9. Top- and cross-sectional view SEM images showing the morphology of Sb_2S_3 thin film absorber layer deposited at temperatures of 260 to 340 ^{o}C onto CdS/FTO/glass substrates.
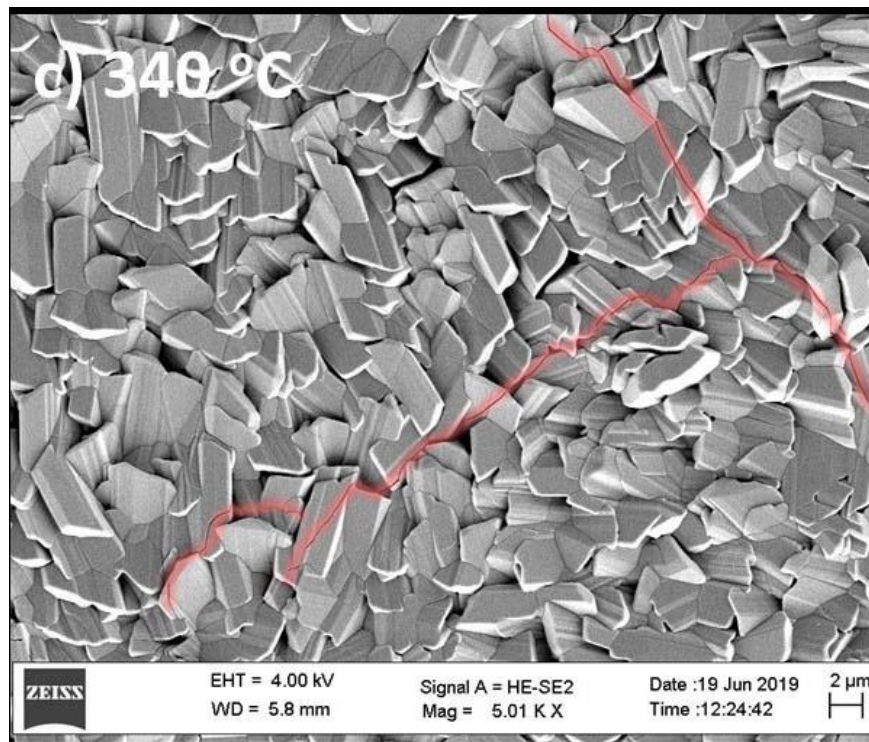
Fig. 10. Top-view SEM images (large scanned area) showing the presence of micro-cracks (highlighted with red color) in Sb_2S_3 thin film absorber layer deposited at 340 ^{o}C.

From thin film growth theory [5] it is known that the cracks in the films are determined by the presence of reactive species in the environments, residual stress, and the precise film stack (i.e., substrate and under layers). Considering the absence of any reactive species in the CSS system, the appearance of the micro-cracks in Sb_2S_3 films deposited 340 °C can be explained as being due to development of compressive stress in the plane of the substrate (in-plane stress), possible originated by a lattice mismatch between the Sb_2S_3 absorber and CdS buffer under layer. Furthermore, the issue of lattice mismatch could be worsen by the difference of thermal expansion coefficients (thermal expansion coefficient mismatch) [27][28] between semiconductor layers in the stack. This could result in bowing, bending or cracking in the Sb_2S_3 on CdS under layer [27][28]. Generally, the thermal expansion decreases with increasing bond energy, which also has an effect on the melting point of solids, so, high melting point materials are more likely to have lower thermal expansion [29]. The melting point of Sb_2S_3 is 550 °C [30] being lower compared to the melting point of Sb_2Se_3 (611°C) [31] PV absorber – a material from antimony chalcogenides family having similar 1D anisotropic lattice structure comprised of "nano-ribbons" and bonded together via Van-der-Waals forces (Figure 2). For the later PV absorber, no cracks have been observed during the CSS deposition in the same interval of temperatures 300-350 °C [4]. Moreover, in contrast with Sb_2S_3, the development of Sb_2Se_3 absorber by CSS required high substrate temperature (450 °C) to obtain compact, pinhole-free and homogeneous layers [4]. Presumably the presence of micro-cracks in Sb_2S_3 films deposited at 340 °C together with local delamination of the absorber from CdS/FTO/glass substrates will have an adverse impact on the solar cell performance.

To gain more insight in the structure of Sb_2S_3 deposited at 260-340 °C, the films were analyzed by XRD. Figure 11 displays the XRD patterns of Sb_2S_3/CdS/FTO/glass heterostructures with Sb_2S_3 absorber deposited at temperatures of 260-340 °C. All the films are polycrystalline, no preferably orientation, and with diffraction peaks corresponding to the orthorhombic Sb_2S_3 crystal structure (PDF card no: 00-042-1393), and generally matching well with those reported in the literature for Sb_2S_3 layers deposited by the CSS and VE techniques [6][7][9]. There were no obvious changes or a clear trend in the orientation, and peak intensities of Sb_2S_3 films as a function of CSS deposition temperature and no secondary phases were detected in the layers. At the same time, continuing parallel with Sb_2Se_3 absorber layers (deposited by CSS in the same order of temperatures) which are always [211] and [221] preferentially oriented films, the diffractogram of Sb_2S_3 (Figure 11) shows a large number of intense (220), (120), (130), (230), (240), (440) XRD peaks with, corresponding to [hkl, l=0] orientation. This sets of XRD peaks are present in all Sb_2S_3 films deposited at

temperature range of 260-340 $^{\circ}$C. More important, only Sb_2S_3 films deposited at 300 $^{\circ}$C exhibit a relatively intense (221) diffraction peak while below this temperature the peak is still present in the diffractogram but with lower intensity. It is known that both, Sb_2S_3 and Sb_2Se_3 have 1D crystal structure [4] and one critical requirement for these PV absorber materials is to preserve the [hkl, l≠0] preferential orientations, where the defined Miller indices l of 1D material is along the chain direction of the layers (Figure 2). This important specification enables an optimal carrier transport through the growth of properly aligned and connected 1D ribbon structures and hence improve the thin film solar cell power conversion efficiency (PCE). One of the critical rules in thin film growth theory follows the principle of minimum energy and suggests that layers parallel to the substrate and bonded through van der Waals forces with the substrate are more thermodynamically favored than the formation of standing layers (perpendicular to the substrate) bonded via covalent bonds with the substrate [5][32][33][34]. Thus the current research efforts and strategies in Sb-based PV technology are oriented towards optimization of various deposition processes to obtain absorber films with [hkl, l≠0] orientation. So far, high PCE Sb_2Se_3, $Sb_2(S,Se)_3$ thin film solar cells have been achieved with [211] and [221] oriented Sb_2Se_3 absorber layer [35], i.e., absorber with large columnar-sintered grains perpendicular to the substrate.

To gain more understanding on the impact of CSS deposition conditions on the microstructural properties of Sb_2S_3 thin films, the changes in the crystallite sizes and lattice parameters of the absorber layers were further investigated. The lattice parameter and crystallite size values are listed in Table 1. The increase of crystallite size follows the similar trend of grain size increase with increasing the CSS deposition temperature, as previously seen by SEM (Figure 9a-c). Thus the crystallite size increased from 96 nm to 110 nm when the substrate temperature was increased from 260 to 340 °C, in agreement with the SEM results. Following the changes in the lattice parameters of Sb_2S_3 films deposited at 260-340 $^{\circ}$C on CdS/FTO/glass substrates it was found that the lattice parameters increases along all a, b and c axes with increasing the CSS substrate temperature. It is also worth to mention that the Sb_2S_3 films had lattice parameters greater compared to Sb_2S_3 powder raw material (Table 1).
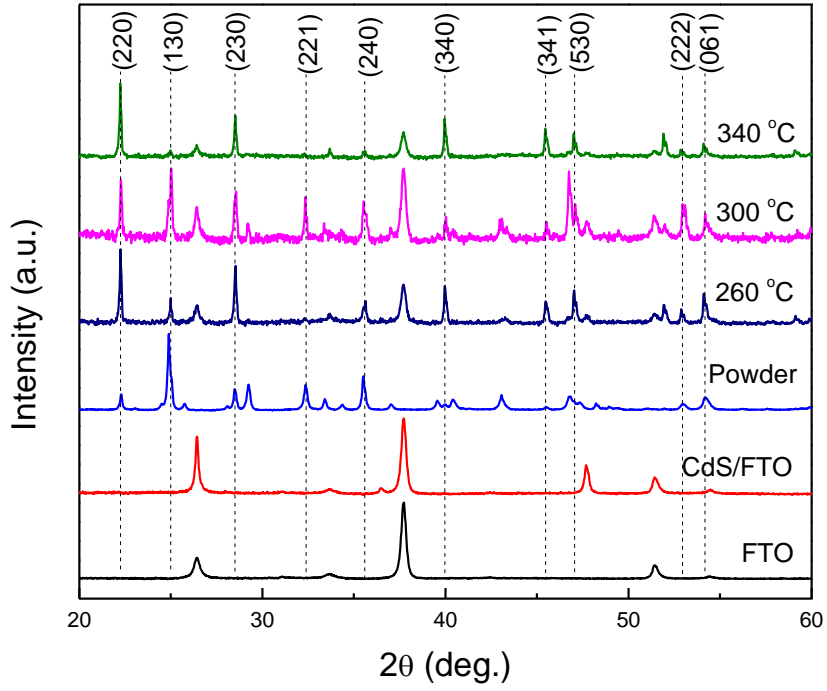
Figure 11. XRD patterns of Sb_2S_3/CdS/FTO/glass structures with Sb_2S_3 absorber films deposited at temperatures between 260 and 340 ºC.

Table 1. Average crystallite size (D) and lattice parameter (a_0) of Sb_2S_3 films deposited at 260-340 ºC onto CdS/FTO/glass substrates. The number in parentheses for a_0 indicates the standard deviation for each value obtained by the least squares refinement.

CSS substrate temperature	D (nm)	Sb_2S_3 (PDF card: 00-042-1393) a_0 (Å)		
		a	b	c
Sb_2S_3 powder raw material	-	11.218(3)	11.269(4)	3.635(4)
260	96 nm	11.226(2)	11.312(6)	3.643(14)
300	97 nm	11.231(5)	11.310(5)	3.640(8)
340	110 nm	11.237(6)	11.314(17)	3.840(8)

A similar case was previously observed in CdTe deposited by CSS at 250-500 ^{o}C that was explained by compressive strain due to the lattice mismatch between CdTe and CdS. Although CdTe has a cubic structure with a single lattice parameter, this explanation could be valid also for low-symmetry Sb_2S_3 orthorhombic structure with three lattice parameters. The low lattice parameter of Sb_2S_3 deposited at 260 ^{o}C can be related to the highly defective structure of the absorber grown at this temperature. The small lattice parameter indicates the presence of vacancy-type defects, which their concentration decreases with increasing substrate temperature.

3.2 Impact of CSS deposition temperature on the Sb_2S_3/CdS thin film solar cells performance

Figure 12 shows the current–voltage (J–V) characteristics measured under AM1.5 conditions for Au/Sb_2S_3/CdS/FTO/glass thin film solar cells with Sb_2S_3 absorber grown at substrate temperatures between 260-340 °C. The evolution of photovoltaic (PV) parameters, including the open-circuit voltage (V_{OC}), fill factor (FF), short-circuit current density (J_{SC}), and PCE as a function of CSS deposition conditions is shown in Figure 13.
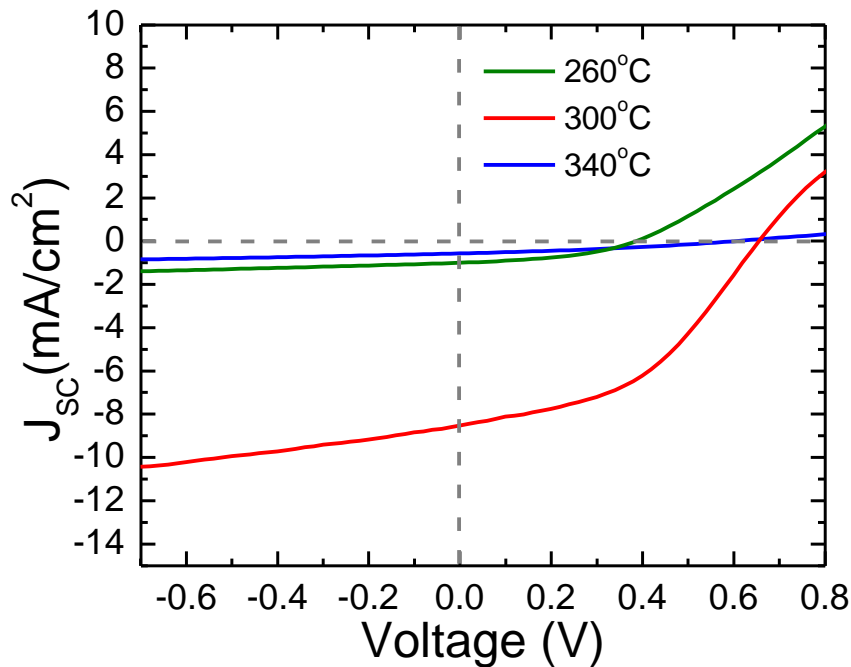
Figure 12. Current-voltage characteristics of the Au/Sb_2S_3/CdS/FTO/glass thin film solar cells with Sb_2S_3 absorber deposited at temperatures of 260-340 °C.

As can be seen in the figure 12 and 13 the PV parameters of the solar cells are strongly affected by the CSS deposition temperature of the Sb_2Se_3 absorber layer. The solar cells with Sb_2Se_3 obtained at substrate temperature of 260 °C exhibit V_{OC}, J_{SC}, FF, and PCE of 385 mV, 1.1 mA/cm^2, 43%, and 0.15%, respectively. The maximum value of PV parameters and PCE was obtained for the solar cell devices with absorber film deposited at 300 °C, showing V_{OC}, J_{SC}, FF and PCE of 650 mV, 8.5 mA/cm^2, 45%, and 2.5%, respectively. For the devices with the absorber grown at 340 °C, all the PV parameters and consequently the PCE decreases drastically achieving the lowest PCE of 0.3%. It should be noticed that for the last temperature, the dramatically decrease of the PCE was strongly determined by the abrupt drop of J_{SC} from 8.5 mA/cm^2 to 1.5 mA/cm^2 and FF from 45% to 34%, whereas a slight decrease of the V_{OC} from 650 to 590 was observed. In contrast, the low PCE of solar cells obtained at 260 °C was largely determined by an abrupt drop in the V_{OC} with the lowest value of 385 mV.
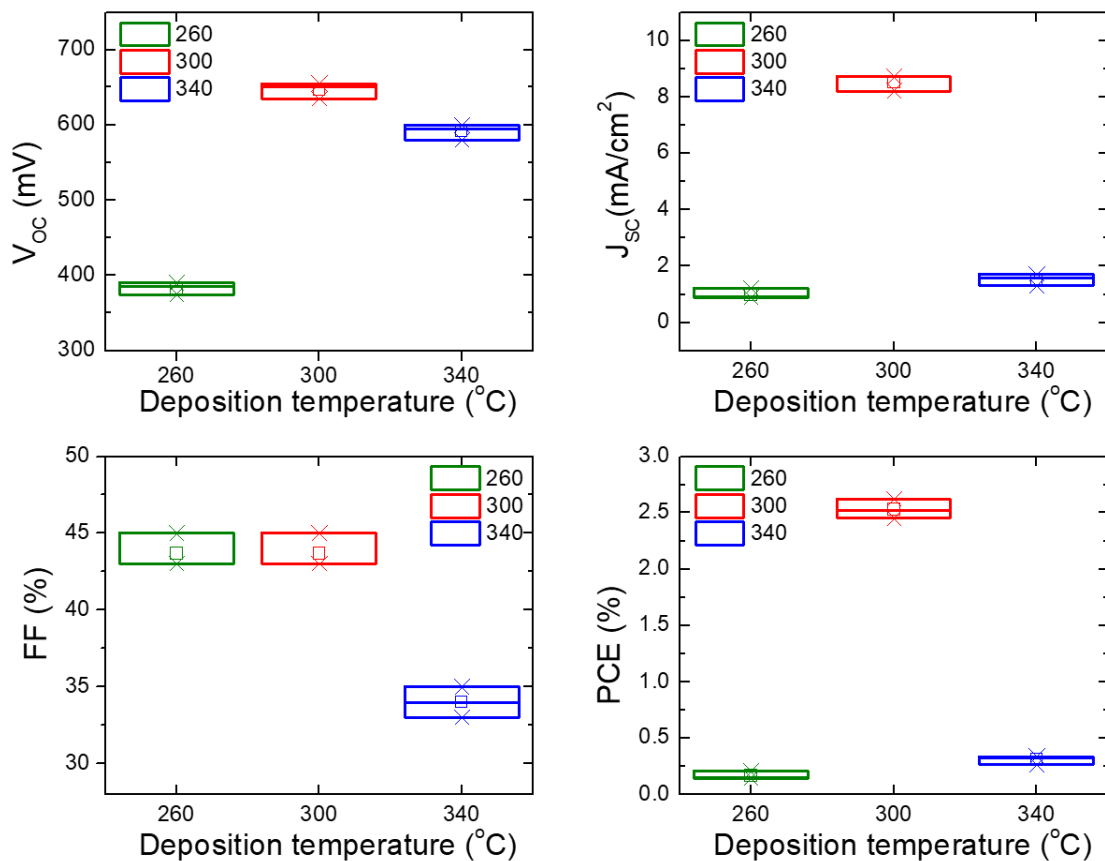
Figure 13. Evolution of PV parameters, V_{OC}, J_{SC}, FF, and PCE (extracted from current-voltage characteristics Figure 12) of Au/Sb_2S_3/CdS/FTO/glass thin film solar cells depending on CSS deposition temperature (260-340 °C) of Sb_2S_3 absorber layer.

The PCE trend is supported by systematic changes in the short and long-wavelength regions of the EQE (Figure 14). The EQE response of solar cell devices with the Sb_2S_3 absorber grown at 260 °C and 340 °C was low through the entire wavelength range (300-800 nm) following the J_{SC} tendency (Figure 13). Following the current density trend and the best PCE, the maximum EQE response was obtained for the solar cells processed at 300 °C.
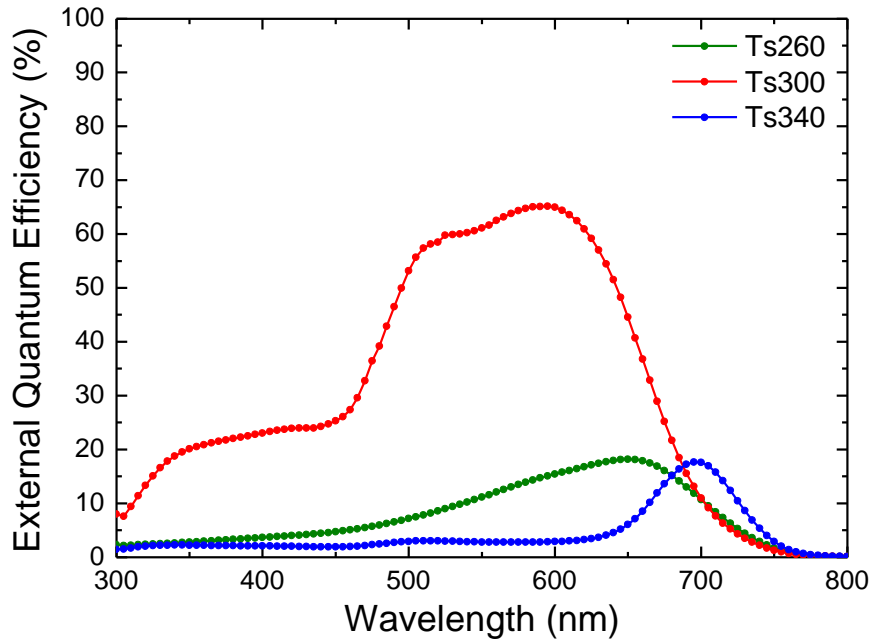
Figure 14. External quantum efficiency (EQE) spectra of Au/Sb₂S₃/CdS/FTO/glass thin film solar cells with Sb₂S₃ absorber deposited at 260-340 °C.

When explaining the impact of CSS deposition temperature on the Au/Sb₂S₃/CdS/FTO/glass solar cell device performance, the changes in the structural defects and optoelectronic properties of Sb_2S_3 absorber layers deposited at different temperatures, 260-340 °C should be considered. It is known from other chalcogenide PV technologies (such as CdTe, CIGS, SnS, Sb_2Se_3, etc.) that the grain morphology, grain size and grain boundaries (GBs) have a major effect on the device efficiency [4][24][25][26][36]. In particular, for CdTe (3D crystal structure material) and Sb_2Se_3 (1D material) absorber layers developed by CSS it was shown that the small grains lead to lower PCE [4][5][36]. This happens because the small grains in the films leads to high density of GBs, the latter tend to be recombination active, which lowers the photo generated minority carrier lifetime. GBs also increase the number of scattering sites for carriers, which reduces carrier mobility. Recombination also leads to an increased dark current (I_O), which reduces V_{OC} according to the equation (4), where n - ideality factor

and I_L = illuminated current (photocurrent). Thus the V_{OC} is practically a measure of the amount of recombination in the device. Even though the recombination is the main limitation factor, the V_{OC} is also strongly determined by the carrier concentration in the absorber (as well as the carrier density in the junction partner layer), according to the equation (5). Where kT/q is the thermal voltage, N_A is the doping concentration (acceptor), Δn is the excess carrier concentration under illumination, and n_i is the intrinsic carrier concentration. The minority carrier mobility or carrier lifetime ultimately impact the collection length in a solar cell device (Eq. 6). The last parameter has a strong effect also on J_{SC}, as the minority carrier diffusion length improves (or decrease), the carriers are efficiently collected (or lost by recombination, respectively) having a direct effect on J_{SC}.

$$V_{OC} = \frac{nkT}{q}\ln\left(\frac{I_L}{I_O} + 1\right) \ (4) \quad V_{OC} = \frac{kT}{q}\ln\left[\frac{(N_A+\Delta n)\Delta n}{n_i^2}\right] (5) \qquad L \sim \sqrt{\mu\tau} \ (6)$$

Considering these approaches, the low V_{OC} and hence limited PCE of Sb_2S_3/CdS solar cells with Sb_2S_3 absorber obtained at 260 °C are clearly determined by the highly dispersed thin film absorber structure with, small grains, high density of GBs as seen by SEM (Figure 9). This argument is also being supported from XRD results (Figure 10) where the diffractogram for 260 °C deposition temperature interval showed a large number of intense (hk0) peaks and very low intensity (221) peak. This suggests that the most of Sb_2S_3 grains are likely to lye parallel on the substrates and thus, the photo generated carriers must jump against inter-grain barriers, causing carrier transport difficulty before reaching the back contact (Au). This results in short carrier diffusion length, low carrier mobility and inefficient charge collection thereby decreasing the J_{SC}, PCE and EQE response (Figures 13, 14). In contrast, SEM and XRD results of Sb_2S_3 absorber layers deposited at 300 °C on CdS/FTO/glass revealed films with sintered grains, low density of GBs and pronounced (221) XRD peak. This means that the majority of grains in the films are aligned perpendicular to the substrate CdS/FTO/glass stack, causing longer diffusion length, efficient carrier collection (highest EQE response, Figure 14) and consequently higher PCE solar cell device (Figures 13, 14). Following the same argument, the XRD and SEM results of hetero-structures with Sb_2S_3 absorber obtained at 340 °C showed films with [hk0] orientation, compact large grains, but also having cracks. This has effects in the device performance by slow drop in the V_{OC}, sudden fall of the J_{SC} (consequently low EQE in Figure 14) since the cracks acts as microdefects which causes power losses in solar cell by providing an alternate current path for the light-generated current (leakage current).

So far the best PCE of 2.5% has been obtained for Au/Sb_2S_3/CdS/FTO/glass solar cells device with Sb_2S_3 absorber deposited at 300 °C indicating that this is the optimal grain growth protocol for CSS technique. Although a promising result, the PCE of this novel Sb_2S_3 based device is still lower compared to its similar Sb_2Se_3 match. The great shortage in the J_{SC} remains a great challenge for Sb_2S_3 based solar cell. As shown above, the PV device parameters, J_{SC} and V_{OC} are strongly influenced by carrier diffusion length and charge collection (Eq. 4-6). From the theory of solar cells, it is also known that the width of the space charge region (SCR) play also a critical role in the device performance [36][37]. The width of the SCR in a p−n heterojunction depends on many parameters, but among these, the carrier concentration is crucial in both p-type absorber as well as in n-type junction partner layer. Generally, the SCR is virtually located in the absorber layer which has a low carrier concentration. For example, in CdTe and CIGS thin film solar cells, where the p−n junction is formed between the n-type (TCO)/CdS window-buffer and the p-type absorber, the SCR extends mainly in the absorber material with a higher resistivity and a lower carrier concentration (low doping level, $10^{14}-10^{16}$ cm^{-3}) than those of the n-type partner ($10^{18}-10^{20}$ cm^{-3}) [36][37]. Such configuration provides a major advantage since the absorption starts in the SCR, which is the main active region where the photo generated electron−hole pairs are effectively separated, giving rise to the short-circuit current and voltage [36][37]. The carrier density in CSS CdTe films usually reach the level of $10^{14}-10^{16}$ cm^{-3} only after halide treatments (CdCl^2, MgCl^2) [5][32] and group V doping (As, P, Sb, Bi) [5] while before these post deposition processing methods the films show extremely high resistivity ($\rho \geq 10^{10}$ Ω·cm) and consequently very low carrier density [5][32]. In comparison with CdTe, the untreated and undoped CSS Sb_2Se_3 absorber layers have lower resistivity ~10^6 Ω·cm and carrier density about 10^{14} cm^{-3}. Although both these materials show similar configuration of intrinsic deep point defects (V_{Cd} and V_{Sb} in CdTe and Sb_2Se_3, respectively), the difference in the electrical properties originate from deferred nature of these materials. CdTe has 3D crystal structure and dangling bonds at the interface between grains (compromising carrier lifetime), whereas the Sb_2Se_3 has 1D lattice structure comprised of "nano-ribbons", thus minimizing the existence of breaking bonds at the GBs, making Sb_2Se_3 GB defect tolerant. Coming back to Sb_2S_3 absorber layers developed in this work, the resistivity of the films was measured by Van der Paw method and estimated to be ~10^8 Ω·cm. This value is two order of magnitude higher than of CSS Sb_2Se_3 thin films obtained in related studies [4], implying that the carrier density in Sb_2S_3 is at least 2 orders of magnitude lower than in Sb_2Se_3. This result together with un-optimal grain orientation of Sb_2S_3 absorber (compared to Sb_2Se_3) explain the high shortage in the J_{SC} and PCE of Sb_2S_3/CdS device. Following the achieved 3% efficiency of Au/Sb_2S_3/CdS/FTO/glass the superstrate configuration solar cells substantial room remains for device improvement.

This improvement may involve, more controllable growth via seed layer screening, various post-deposition treatments (halide treatments, selenization) as well as adoption of doping strategies.

CONCLUSIONS

The main focus of the the study was to gain insight on the novel Sb_2S_3 thin film solar cell and to investigate the effect of different CSS substrate temperature on Sb_2S_3 solar cell performance. The study led to obtaining more information on solar cells working principle, as well as different deposition and characterization techniques, and also deep knowledge on Sb_2S_3 absorber layer. The properties of Sb_2S_3 were investigated by means of XRD, SEM, EDX, van der Pauw and EQE methods. The results of the study are as follows:

1) Sb_2S_3 grain shape and grain size have a strong dependence on the substrate temperature; the grain size increased when the temperature raised from 260 °C to 340 °C. Also the GBs defects that once were observed in lower temperature in the absorber material, started to become much less when the temperature increased. Several micro crack were observed during investigation of samples that were deposited at 340 °C, due to existence of compressive stress in the substrate plane.

2) The diffractogram of Sb_2S_3 deposited at 260 °C shows a large number of intense (220), (120), (130), (230), (240), (440) XRD peaks-an indication of the grains lying on the CdS/FTO substrate. XRD of Sb_2S_3 deposited at 300 °C showed intense (221) peak, indication of columnar grain growth.

3) Crystallite sizes and lattice parameters changes of the absorber layers also were observed. The crystallite size increased from 96 nm to 110 nm along with substrate temperature rise from 260 to 340 °C. Furthermore, the lattice parameters of Sb_2S_3 films increased along all a, b and c axes.

4) The current–voltage (J–V) characteristics of the solar cells with Sb_2S_3 absorber deposited at 260-340 °C were measured under AM1.5 conditions. In general, with increasing the substrate temperature from 260 to 300 °C, the V_{OC}, J_{SC}, FF, and PCE parameters increased, while by increasing the temperature to 340 °C, these parameters decreased drastically achieving the lowest PCE of 0.3%. The maximum value of PV parameters and PCE was obtained for the solar cell devices with absorber film deposited at 300 °C, showing V_{OC}, J_{SC}, FF and PCE of 650 mV, 8.5 mA/cm^2, 45%, and 2.5%, respectively.

5) In 300 °C substrate temperature, Sb_2S_3 showed large grains, perpendicular to the substrate, resulting in increased diffusion length, efficient carrier collection and higher PCE followed by increase in the J_{SC} and EQE. The great deficiency in the J_{SC} remains a great challenge for Sb_2S_3 based solar cell, most probably due to the high resistivity (10^8 Ω·cm) and consequently low carrier density in the absorber. Further systematic investigations are necessary to improve the J_{SC} and

efficiency of Sb_2S_3 based solar cells, such as controllable growth via seed layer screening, various post-deposition treatments (halide treatments, selenization) as well as adoption of doping strategies might be as importance.

SUMMARY

Global warming and upcoming changes in the earth average temperature, are major concerns which need to be considered as high priority in the current century. There are many technologies working towards solving the mentioned issues, among them green energy technologies. Between all the green energy sources, solar power and specifically Photovoltaics (PVs) are one of the cleanest and most favorable energy kind to be used. So far, silicon based solar cells have the greatest share in the market due to their high efficiency compared to other PV technologies,but their high cost is a great barrier. Thin film solar cells, on the contrary, use less material and has low-cost comparing to silicon solar cells. Between all the thin film absorbers, Sb_2S_3 is recognized a non-toxic and stable material.

This study is based on Sb_2S_3 absorber material deposition by CSS technology. The aim of the research is to investigate the effect of different substrate temperatures on the properties of Sb_2S_3 thin films and Sb_2S_3/CdS solar cell performance.

Sb_2Se_3 films with small grains and high density of grain boundaries were obtained at 260 °C, while compact layers were grown at 300 and 340 °C. For the later temperature, micro-cracks were detected on the surface of the films. XRD result showed a large number of (120), (130), (230) peaks for the films deposited at 260 and 340 °C - an indication of the grains lying on the CdS/FTO substrate. XRD of Sb_2S_3 deposited at 300 °C showed intense (221) peak, indication of columnar grain growth. Evolution of the lattice parameter depending on the deposition temperature indicated presence of in-plane stress in the films, emphasised in the layers grown at 340 °C. The best PV parameters and efficiency of 2.5% was obtained for the solar cell with Sb_2S_3 deposited at 300 °C, having dense columnar grains. Low PCE of 0.15% and 0.3% were achieved for the devices with highly defective Sb_2S_3 films obtained at 260 °C and cracked Sb_2S_3 layers at 340 °C, respectively.

There's still much to be done for improvement of Sb_2S_3 solar cell performance and properties. Further studies need to be carried out, in order to solve the current issues and achieve better efficiencies in this material. Growth control, post-deposition treatments and doping are recommended for the objective.

REFERENCES

[1] IRENA, G.E.T., 2018. A Roadmap to 2050. Abu Dhabi: International Renewable Energy Agency.

[2] J. Rogelj, M. D. Elzen, N. Höhne, T. Fransen, H. Fekete, H. Winkler, R. Schaeffer, F. Sha, K. Riahi, and M. Meinshausen, "Paris Agreement climate proposals need a boost to keep warming well below 2 °C," *Nature*, vol. 534, no. 7609, pp. 631–639, 2016.

[3] M. Üürike, Influence of pH on the properties of chemically deposited CdS thin films and solar cells, Tallinn: TUT Press, 2017.

[4] R. Krautmann, Development of Sb_2Se_3 Thin Film Solar Cells By Close-Spaced Sublimation,Tallinn: TUT Press, 2019.

[5] N. Spalatu, Development of CdTe Absorber Layer for Thin-Film Solar Cells, Tallinn: TUT Press, 2017.

[6] L. Guo, B. Zhang, S. Li, Q. Zhang, M. Buettner, L. Li, X. Qian, and F. Yan, "Scalable and efficient Sb_2S_3 thin-film solar cells fabricated by close space sublimation," *APL Materials*, vol. 7, no. 4, p. 041105, 2019.

[7] R. Kondrotas, C. Chen, and J. Tang, "Sb_2S_3 Solar Cells," *Joule*, vol. 2, no. 5, pp. 857–878, 2018.

[8] M. Y. Versavel and J. A. Haber, "Structural and optical properties of amorphous and crystalline antimony sulfide thin-films," *Thin Solid Films*, vol. 515, no. 18, pp. 7171–7176, 2007.

[9] P. K. Nair, González-Lua Rogelio, Rodríguez Manuela Calixto, Martínez Jesús Capistrán, O. Gomezdaza, and M. T. S. Nair, "Antimony Sulfide Absorbers in Solar Cells," 2011.

[10] X. Wang, R. Tang, C. Wu, C. Zhu, and T. Chen, "Development of antimony sulfide–selenide $Sb_2(S, Se)_3$-based solar cells," *Journal of Energy Chemistry*, vol. 27, no. 3, pp. 713–721, 2018.

[11] Y. Zeng, F. Liu, M. Green, and X. Hao, "Fabrication of Sb_2S_3 planar thin film solar cells with closed-space sublimation method," *2018 IEEE 7th World Conference on Photovoltaic Energy Conversion (WCPEC) (A Joint Conference of 45th IEEE PVSC, 28th PVSEC & 34th EU PVSEC)*, 2018.

[12] S. Messina, M. Nair, and P. Nair, "Antimony sulfide thin films in chemically deposited thin film photovoltaic cells," *Thin Solid Films*, vol. 515, no. 15, pp. 5777–5782, 2007.

[13] J. S. Eensalu, A. Katerski, E. Kärber, I. O. Acik, A. Mere, and M. Krunks, "Uniform Sb_2S_3 optical coatings by chemical spray method," *Beilstein Journal of Nanotechnology*, vol. 10, pp. 198–210, 2019.

[14] A. Abbas, D. Meysing, M. Reese, T. Barnes, J. Walls, and C. Wolden, "Structural and chemical evolution of the CdS:O window layer during individual CdTe solar cell processing steps," *Solar Energy*, vol. 159, pp. 940–946, 2018.

[15] N. Amin and K. S. Rahman, "Close-Spaced Sublimation (CSS): A Low-Cost, High-Yield Deposition System for Cadmium Telluride (CdTe) Thin Film Solar Cells," *Modern Technologies for Creating the Thin-film Systems and Coatings*, Aug. 2017.

[16] A. Seth, G. Lush, J. Mcclure, V. Singh, and D. Flood, "Growth and characterization of CdTe by close spaced sublimation on metal substrates," *Solar Energy Materials and Solar Cells*, vol. 59, no. 1-2, pp. 35–49, 1999.

[17] C. Ferekides, J. Britt, Y. Ma, and L. Killian, "High efficiency CdTe solar cells by close spaced sublimation," *Conference Record of the Twenty Third IEEE Photovoltaic Specialists Conference - 1993 (Cat. No.93CH3283-9)*.

[18] B. Inkson, "Scanning electron microscopy (SEM) and transmission electron microscopy (TEM) for materials characterization," *Materials Characterization Using Nondestructive Evaluation (NDE) Methods*, pp. 17–43, 2016.

[19] A. L. V. D. Ven, A. Mack, K. Dunner, M. Ferrari, and R. E. Serda, "Preparation, Characterization, and Cellular Associations of Silicon Logic-Embedded Vectors," *Methods in Enzymology Nanomedicine - Cancer, Diabetes, and Cardiovascular, Central Nervous System, Pulmonary and Inflammatory Diseases*, pp. 1–16, 2012.

[20] J. Epp, "X-ray diffraction (XRD) techniques for materials characterization," *Materials Characterization Using Nondestructive Evaluation (NDE) Methods*, pp. 81–124, 2016.

[21] R. Kohli, "Methods for Monitoring and Measuring Cleanliness of Surfaces," *Developments in Surface Contamination and Cleaning*, pp. 107–178, 2012.

[22] N. Ngo, H. Niu, P. Bharadwaj, H. Bhatti, and S. Adhikari," Van der Pauw Resisitivity Measurement", *Technical Report*, 2017.

[23] T. Markvart and L. Castañer, "Principles of Solar Cell Operation," *McEvoys Handbook of Photovoltaics*, pp. 3–28, 2018.

[24] N. Spalatu, M. Krunks, and J. Hiie, "Structural and optoelectronic properties of $CdCl_2$ activated CdTe thin films modified by multiple thermal annealing," *Thin Solid Films*, vol. 633, pp. 106–111, 2017.

[25] T. Potlog, N. Spalatu, N. Maticiuc, J. Hiie, V. Valdna, V. Mikli, and A. Mere, "Structural reproducibility of CdTe thin films deposited on different substrates by close space sublimation method," *physica status solidi (a)*, vol. 209, no. 2, pp. 272–276, 2011.

[26] N. Spalatu, J. Hiie, V. Mikli, M. Krunks, V. Valdna, N. Maticiuc, T. Raadik, and M. Caraman, "Effect of $CdCl_2$ annealing treatment on structural and optoelectronic properties of close spaced sublimation CdTe/CdS thin film solar cells vs deposition conditions," *Thin Solid Films*, vol. 582, pp. 128–133, 2015.

[27] C. K. Gan, J. R. Soh, and Y. Liu, "Large anharmonic effect and thermal expansion anisotropy of metal chalcogenides: The case of antimony sulfide," *Physical Review B*, vol. 92, no. 23, Feb. 2015.

[28] T. Y. Tsui, A. J. Mckerrow, and J. J. Vlassak, "Constraint Effects on Thin Film Channel Cracking Behavior," *Journal of Materials Research*, vol. 20, no. 9, pp. 2266–2273, 2005.

[29] A. K. Varshneya and J. C. Mauro, "Fundamentals of inorganic glass making," *Fundamentals of Inorganic Glasses*, pp. 631–685, 2019.

[30] W. M. Haynes, "CRC Handbook of Chemistry and Physics, 95th Edition," Apr. 2014.

[31] K. Li, C. Chen, S. Lu, C. Wang, S. Wang, Y. Lu and J. Tang, "Orientation Engineering in Low-Dimensional Crystal-Structural Materials via Seed Screening," Advanced Materials, 2019.

[32] J. Major and K. Durose, "Early stage growth mechanisms of CdTe thin films deposited by close space sublimation for solar cells," *Solar Energy Materials and Solar Cells*, vol. 95, no. 12, pp. 3165–3170, 2011.

[33] Eckertova, L., „Physics of Thin Films" second ed1986.

[34] Petrov, I., Barna, P.B., Hultman, L. and Greene, J.E., 2003. Microstructural evolution during film growth. Journal of Vacuum Science & Technology A: Vacuum, Surfaces, and Films, 21(5), pp.S117-S128.

[35] O. S. Hutter, L. J. Phillips, K. Durose, and J. D. Major, "6.6% efficient antimony selenide solar cells using grain structure control and an organic contact layer," *Solar Energy Materials and Solar Cells*, vol. 188, pp. 177–181, 2018.

[36] N. Spalatu, J. Hiie, R. Kaupmees, O. Volobujeva, J. Krustok, I. O. Acik, and M. Krunks, "Postdeposition Processing of SnS Thin Films and Solar Cells: Prospective Strategy To Obtain Large, Sintered, and Doped SnS Grains by Recrystallization in the Presence of a Metal Halide Flux," ACS Applied Materials & Interfaces, vol. 11, no. 19, pp. 17539–17554, 2019.

[37] A. Reinders, P. Verlinden, W. Van Sark, and A. Freundlich, "Advanced Module Concepts," *Photovoltaic Solar Energy*, pp. 502–510, Jul. 2017.